Exploring the ATN classification system using Brain Morphology

Nils Heinzinger[1,2], Anne Maass[1,2], David Berron[1,2], Renat Yakupov[1,2], Oliver Peters[3,4], Jochen Fiebach[29], Kersten Villringer[29], Lukas Preis[4], Josef Priller[3,5,27,28], Eike Jacob Spruth[3,5], Slawek Altenstein[3,5], Anja Schneider[6,7], Klaus Fliessbach[6,7], Jens Wiltfang[9,10,25], Claudia Bartels[10], Frank Jessen[6,11,24], Franziska Maier[11], Wenzel Glanz[1], Katharina Buerger[12,13], Daniel Janowitz[13], Martin Dichgans[12,13], Robert Perneczky[12,18,19,20], Boris-Stephan Rauchmann[18], Stefan Teipel[14,15], Ingo Killimann[14,15], Doreen Göerß[15], Christoph Laske[16,17], Matthias H. Munk[16,17], Annika Spottke[6,8], Nina Roy[6], Michael T. Heneka[6,7], Frederic Brosseron[6,7], Laura Dobisch[1], Michael Ewers[12], Peter Dechent[21], John Dylan Haynes[22], Klaus Scheffler[23], Steffen Wolfsgruber[6,7], Luca Kleineidam[6], Matthias Schmid[6,26], Moritz Berger[26], Emrah Düzel[1,2,*], Gabriel Ziegler[1,2,*]

** Shared last-authorship, [1] German Center for Neurodegenerative Diseases (DZNE), Magdeburg, Germany, [2] Institute of Cognitive Neurology and Dementia Research (IKND), Otto-von-Guericke University, Magdeburg, Germany, [3] German Center for Neurodegenerative Diseases (DZNE), Berlin, Germany, [4] Charité-Universitätsmedizin Berlin, Campus Benjamin Franklin, Department of Psychiatry, Berlin, Germany, [5] Department of Psychiatry and Psychotherapy, Charité, Berlin, Germany, [6] German Center for Neurodegenerative Diseases (DZNE), Bonn, Germany, [7] University of Bonn Medical Center, Dept. of Neurodegenerative Diseases and Geriatric Psychiatry/Psychiatry, Bonn, Germany, [8] Department of Neurology, University of Bonn, Bonn, Germany, [9] German Center for Neurodegenerative Diseases (DZNE), Göttingen, Germany, [10] Department of Psychiatry and Psychotherapy, University Medical Center Göttingen, University of Göttingen, Göttingen, Germany, [11] Department of Psychiatry, University of Cologne, Medical Faculty, Cologne, Germany, [12] German Center for Neurodegenerative Diseases (DZNE), Munich, Germany, [13] Institute for Stroke and Dementia Research (ISD), University Hospital, LMU Munich, Munich, Germany, [14] German Center for Neurodegenerative Diseases (DZNE), Rostock, Germany, [15] Department of Psychosomatic Medicine, Rostock University Medical Center, Rostock, Germany, [16] German Center for Neurodegenerative Diseases (DZNE), Tübingen, Germany, [17] Section for Dementia Research, Hertie Institute for Clinical Brain Research and Department of Psychiatry and Psychotherapy, University of*

Tübingen, Tübingen, Germany, [18] Department of Psychiatry and Psychotherapy, University Hospital, LMU Munich, Munich, Germany, [19] Munich Cluster for Systems Neurology (SyNergy), Munich, Germany, [20] Ageing Epidemiology Research Unit (AGE), School of Public Health, Imperial College London, London, UK, [21] MR-Research in Neurosciences, Department of Cognitive Neurology, Georg-August-University Göttingen, Germany, [22] Bernstein Center for Computational Neuroscience, Charité-Universitätsmedizin, Berlin, Germany, [23] Department for Biomedical Magnetic Resonance, University of Tübingen, Tübingen, Germany, [24] Excellence Cluster on Cellular Stress Responses in Aging-Associated Diseases (CECAD), University of Cologne, Cologne, Germany, [25] Neurosciences and Signaling Group, Institute of Biomedicine (iBiMED), Department of Medical Sciences, University of Aveiro, Aveiro, Portugal, [26] Institute for Medical Biometry, University Hospital Bonn, Bonn, Germany, [27] School of Medicine, Technical University of Munich, Department of Psychiatry and Psychotherapy, Munich, Germany, [28] University of Edinburgh and UK DRI, Edinburgh, UK, [29] Center for Stroke Research Berlin, Charité-Universitätsmedizin, Berlin, Germany

(c) Correspondence to: Nils Heinzinger; Institute for Cognitive Neurology and Dementia Research; University Hospital Magdeburg, University of Magdeburg, Leipziger Str. 44, 39120 Magdeburg, Germany; Email: nils.heinzinger@st.ovgu.de

Alzheimer's Research & Therapy keywords: MRI, Alzheimer’s disease, memory, Voxel-based Morphometry, VBM, ATN, biomarker, Amyloid

Word count for paper: 6056

Word count for abstract: 350

Character count for title: 62

Number of references: 80

Number of tables: 3

Number of figures: 6

Supplementary data:

Number of tables: 2

Number of figures: 4

Abstract

Background: The NIA-AA proposed Amyloid-Tau-Neurodegeneration (ATN) as a classification system for AD biomarkers. The Amyloid Cascade Hypothesis (ACH) implies a sequence across ATN groups that patients might undergo during transition from healthy towards AD: A-T-N-→A+T-N-→A+T+N-→A+T+N+. Here we assess the evidence for monotonic brain volume decline for this particular (Amyloid-conversion first, Tau-conversion second, N-conversion last) and alternative progressions using Voxel-based Morphometry (VBM) in a large cross-sectional MRI cohort.

Methods: We used baseline data of the DELCODE cohort of 437 subjects (127 Controls, 168 SCD, 87 MCI, 55 AD patients) which underwent lumbar puncture, MRI scanning and neuropsychological assessment. ATN classification was performed using CSF-Aβ42/Aβ40 (A+/-), CSF-phospho-Tau (T+/-), and adjusted hippocampal volume or CSF-total-Tau (N+/-). We compared voxel-wise model evidence for monotonic decline of gray matter volume across various sequences over ATN groups using the Bayesian Information Criterion (including also ROIs of Braak stages). First, face validity of the ACH transition sequence A-T-N-→A+T-N-→A+T+N-→A+T+N+ was compared against biologically less plausible (permuted) sequences among AD-continuum ATN groups. Second, we evaluated evidence for 6 monotonic brain volume progressions from A-T-N- towards A+T+N+ including also non-AD-continuum ATN groups.

Results: The ACH-based progression A-T-N-→A+T-N-→A+T+N-→A+T+N+ was consistent with cognitive decline and clinical diagnosis. Using hippocampal volume for operationalization of neurodegeneration (N), ACH was most evident in 9% of gray matter predominantly in the medial temporal lobe. Many cortical regions suggested alternative non-monotonic volume progressions over ACH progression groups, which is compatible

with an early amyloid-related tissue expansion or sampling effects e.g. due to brain-reserve. Volume decline in 65% of gray matter was consistent with a progression where A status converts before T or N status (i.e. ACH/ANT) when compared to alternative sequences (TAN/TNA/NAT/NTA). Brain regions earlier affected by Tau tangle deposition (Braak stage I-IV, MTL, limbic system) present stronger evidence for volume decline than late Braak-stage ROIs (V/VI, cortical regions). Similar findings were observed when using CSF-total-Tau for N instead.

Conclusion: Using the ATN classification system, early Amyloid status conversion (before Tau and Neurodegeneration) is associated with brain volume loss observed during AD progression. The ATN system and the ACH are compatible with monotonic progression of MTL atrophy.

DRKS00007966, 04/05/2015, retrospectively registered

Introduction

Alzheimer's disease (AD) is a slowly evolving neurodegenerative condition where initial brain changes can be found up to decades before the clinical onset and ultimately result in progredient cognitive decline and brain atrophy often studied with Magnetic Resonance Imaging (MRI)[1-3].

AD is characterized by the accumulation of protein deposits, i.e. β-Amyloid plaques and neurofibrillary tangles (NFT) consisting of hyperphosphorylated Tau which can be assessed using cerebrospinal fluid (CSF) biomarkers[4,5]. A reliable marker reflecting Amyloid deposition is the Aβ42/Aβ40 ratio which decreases with increasing deposition[6]. Accumulation of Tau tangles is mirrored by increasing CSF hyperphosphorylated Tau, while CSF total Tau has been more generally associated with neuronal loss, not necessarily AD specific. Those biomarkers have shown potential for predicting the clinical diagnostic conversions[7-9] and worsening of memory performance during disease progression[10].

One key concept about the disease progress and pathological timeline has been introduced as the Amyloid Cascade Hypothesis (ACH)[11-13,1]. Due to different predispositions, including age[14], genes[15] or vascular risk factors[16], ß-Amyloid is increasingly formed from precursor proteins which leads to its aggregation in the brain. Then, ß-Amyloid can induce hyperphosphorylation and malformation/misfolding of intracellular Tau proteins, which aggregate in forms of NFTs[13]. Increased cellular stress results in neuronal loss which typically manifests behaviourally in progressive cognitive decline. Neuronal death in AD manifests in a typical MRI atrophy pattern with strongest morphometrical changes situated in medial temporal lobe (MTL) and other limbic regions, while the primary motor and sensory cortex are often spared[17,18]. Although the ACH was

141 postulated about 30 years ago, the hypothesis is still under refinement and critical
142 review[13,19,20]. Moreover, the stereotypical progression pattern of Tau/NFT spread from
143 the transentorhinal region via the limbic system to the whole cortex during AD progression
144 can be classified into six Braak stages, which have been first described in an autopsy
145 study[5], and later tested in positron emission tomography studies[21,22] or VBM atrophy
146 studies[23].

147 Recently, a new descriptive ATN classification for AD which emphasises pathological and
148 physiological rather than traditional clinical measures such as neuropsychological test
149 scores was proposed[24,25]. In the ATN system, for the three binary categories Amyloid
150 burden, Tau burden and Neurodegeneration, subjects are rated as normal (physiological,
151 "-") or abnormal (pathological, "+"). The resulting 8 (=2^3) groups with different biomarker
152 combinations range from A-T-N- (suggesting no pathology) to A+T+N+ (with pathology in
153 all categories). It has been suggested that all ATN biomarker combinations with A+ reflect
154 a pathological change related to the AD continuum. Several recent studies explored the
155 prognostic possibilities for clinical progression and cognitive decline using ATN[26-30].
156 However, while the ATN classification does not directly imply a progression cascade or a
157 set of subsequently following stages per se, it may be used for this particular purpose.
158 For example, the sequence of a disease transition across pathology groups (1) A-T-N-
159 (2) A+T-N- (3) A+T+N- (4) A+T+N+ is more compatible with the amyloid cascade
160 hypothesis than other progression sequences based on ATN classification groups[25]. If
161 individual participants follow this particular disease progression profile, this would imply
162 a monotonic volume loss across groups (1)→(2)→(3)→(4) in brain areas associated with
163 AD. While above progression sequence is partially supported in selected studies[31,32],
164 those findings are limited to recordings of non-imaging between-group biomarker
165 differences. Although there is evidence for deviating sequences of progression[32], studies

166 focusing on local voxel-based anatomical analysis in relation to ATN groups are still
167 missing (see eg.[33]).

168 Here we study whether above progression implied by the ACH is reflected in specific
169 patterns of local GM volume decline using cross-sectional data from a large neuroimaging
170 cohort (DELCODE; DZNE Longitudinal Cognitive Impairment and Dementia Study) which
171 is well characterized by CSF biomarkers. The DELCODE cohort is specifically enriched
172 in subjects that are at risk for developing AD such as Subjective Cognitive Decline (SCD),
173 but also Mild Cognitive Impairment (MCI) and thus more likely comprises individuals in
174 early preclinical stages of AD (A+).

175 GM volume is a sensitive marker for local brain changes or pathological processes. As
176 this marker is continuous, smallest substance differences for all brain regions can be
177 measured and intermediate changes are detectable even when they would not cause an
178 ATN status conversion. We hypothesize that GM in the hippocampal-network decreases
179 following the ACH sequence and (1) test face validity of an ACH-based sequence using
180 Voxel-based Morphometry without *a-priori* regional assumptions; and (2) compare the
181 evidence for volume loss reflecting the ACH sequence in comparison to other biologically
182 possible progressions outside the AD continuum. Finally, the concordance between ACH
183 progress and Braak staging is evaluated. We expect earlier Braak stages to be stronger
184 affected by atrophy during the ACH sequence. It might occur that the volume alteration is
185 regionally modulated by e.g. reserve mechanisms. Since operationalization might be
186 crucial, we also evaluate the impact of alternative choices for dichotomization of the N
187 category using both t-Tau or hippocampal volume.

188

189 ## Methods

Study Design and Participants

This study uses the baseline data of the DELCODE cohort, an observational multicentre study with 10 sites from the German Centre of Neurodegenerative Diseases (DZNE). Its focus is the multimodal assessment of preclinical stages of dementia of Alzheimer's type (DAT) including SCD, MCI, DAT, and DAT relatives[34]. While SCD, MCI and DAT participants were recruited from memory clinics, relatives of DAT patients and healthy controls were recruited by advertisement and initially screened per phone for self-experienced cognitive decline and memory worries. Further SCD inclusion criteria were a normal cognitive performance (specified as within 1.5 SD compared to an age, sex and education years adjusted control group) in all subtests of the CERAD-plus battery and a MMSE score between 26 and 30 and a CDR score <= 0.5.

Participants with MCI were below 1.5 SD in the CERAD-plus battery, but did not fulfil dementia criteria of NINDCS/ADRDA[35]. Subjects diagnosed as DAT were fulfilling NINDCS/ADRDA criteria, have a CERAD-plus score of below 1.5 SD, and were within an extended MMSE score range of 18-26 and have a CDR rating of >= 1. DAT relatives have a first-grade sibling with diagnosed DAT and do not fulfil MCI or DAT criteria.

Noncomplaining healthy controls (NC) neither suffered from subjective or objective cognitive impairment. All participants were native German speakers, older than 60 years, and gave written informed consent and had a study partner available for consultation. Other neurological or psychiatric disorders than DAT were excluded. More information on study design and inclusion/exclusion criteria can be found elsewhere[34]. DELCODE is retrospectively registered at the German Clinical Trials Register (DRKS00007966), (04/05/2015) and was approved by ethical committees and local review boards. Of a total of 1079 participants at baseline timepoint, we finally included 437 subjects with available

quality checked MRI imaging and CSF biomarkers (see below). Based on a clinical classification approach, this includes 127 NC (including DAT relatives), 168 SCD, 87 MCI and 55 DAT patients. A summary of demographic information of the analysed sample is provided in results table 1.

Neuropsychological testing

In DELCODE, subjects underwent a large battery of neuropsychological tests. Due to our focus on global cognition and memory aspects in healthy and (pre-) clinical DAT patients, we use the Mini Mental State Examination (MMSE, [36]) and a reliable memory composite factor score (further denoted as memory performance). This score was created by Confirmatory Factor Analysis and enables detecting subtle cognitive deviations in SCD when compared to NC subjects[37].

Biomarker and MRI data acquisition

Lumbar puncture was carried out by trained study assistants in 49% of DELCODE participants. CSF samples were centrifuged, aliquoted and stored at -80°C for retests. Biomarkers known to be related to AD pathology (CSF Aβ42, Total Tau, hyperphosphorylated Tau) were determined by commercially available kits (V-PLEX Aβ Peptide Panel 1 (6E10) Kit (K15200E), V-PLEX Human Total Tau Kit (K151LAE) (both Mesoscale Diagnostics LLC, Rockville, USA), Innotest Phospho-Tau(181P) (81581; Fujirebio Germany GmbH, Hannover, Germany)).

MRI scans were acquired in 9 out of 10 involved DZNE sites (3T Siemens scanners: 3 TIM Trio systems, 4 Verio systems, 1 Skyra and 1 Prisma system). Our main analyses were based on whole brain T1-weighted MPRAGE (3D GRAPPA PAT 2, 1 mm^3 isotropic, 256 X 256 px, 192 slices, sagittal, ~5 min, TR 2500 ms, TE 4.33 ms, TI 110 ms, FA 7°). Further ROI and covariate processing was based on additionally available FLAIR and T2-

weighted protocols (for details see[34]). Additional details on standard operation procedures, quality assurance and assessment (QA), performed by the DZNE imaging network (iNET, Magdeburg), can be found elsewhere[34].

Image processing and computational brain morphometry

The MPRAGE images were processed using SPM (SPM12 v7771, Statistical Parametric Mapping software; Wellcome Trust Centre for Human Neuroimaging, London, UK, [38]) and CAT-Toolbox (CAT12.6 r1450, Structural Brain Mapping group, Jena University Hospital, Jena, Germany, [39]) under MATLAB (r2019b, The MathWorks, Inc., Natick, Massachusetts, USA). As first step, a correction for field inhomogeneities was applied. Then the images were segmented into GM, WM and CSF maps using CAT which includes a partial volume estimation correction on AMAP approach[40]. The received tissue maps with a 1 mm isometric voxel size are warped to a study-specific template in MNI space using Geodesic Shooting approach[41]. The GM tissue maps were modulated by the jacobian determinant to enable voxel-based comparisons of local gray matter volume across subjects. A Gaussian blurring kernel was applied with 6 mm full width half maximum (FWHM). The resulting tissue maps were quality tested using CAT's sample homogeneity check and 15 subjects were excluded due to preprocessing artifacts.

For complementary ROI analysis we used Freesurfer's (v6.0, [42]) volume reconstruction (cortical stream[43], subcortical stream[44]) to extract region of interest volumes. This was carried out by the default pipeline initiated by a 'recon-all -all' command which contains all preprocessing steps needed, including for example intensity normalization, surface registration to Talairach space, skull stripping, subcortical segmentation and calculation of affiliated region statistics, WM segmentation, tessellation and inflation of pial parcellated WM surfaces and cortical parcellation with calculation of cortical region

statistics. Four ROIs (amygdala, hippocampus, entorhinal cortex, precuneus), well known to be affected early by AD pathology, were assessed[45-47,17,48]. Furthermore, anatomical masks representing Braak stages were created following[49] and warped to MNI space. Thus, the following cortical regions were included as aggregated volumes: stage I/II: entorhinal cortex and hippocampus, stage III/IV: limbic, insular and temporal regions, V/VI: remaining cortical regions including primary sensory/motor areas or precuneus.

In order to enable a reliable operationalization of the N category of ATN system we used the specifically developed hippocampal segmentation in Freesurfer that is based on a high-resolution T2-weighted scan of the medial temporal lobe[50]. Note, that the obtained hippocampal volumes were only used for the ATN classification of each participant, while all presented voxel-based and ROI volumes were based on conventional CAT and Freesurfer segmentations (as dependent variable). A strong co-occurrence of AD and white matter hyperintensities (WMH) as sign of vascular damage has been reported[16,51-54]. To account for WMH during our analyses, the total lesion volume was extracted using Lesion segmentation toolbox (v3.0.0, LPA and an 0.5 binary threshold, [55,56]).

ATN classification and group comparison

Each participant was classified as normal (-) or abnormal (+) in the Amyloid (A) and Tau (T) category depending on their biomarker levels of Aβ42over40 and phospho-Tau181 respectively. Cut-offs were estimated by a ROC analysis and Youden's index (A = 0.09, T = 57 pg/ml; [34]). In this study we explored effects of two different choices for the neurodegeneration (N) category. We focused on (1) adjusted hippocampal volume (denoted as aHV; cut-off = 2821.1 µl) and (2) CSF Total Tau (cut-off = 470 pg/ml). aHV was derived from the Freesurfer segmentation (see above) and corrected for age, sex, education, total intracranial volume (TICV) and WMH using a linear regression model.

Dichotomization of participants' aHV into N- and N+ was performed using Gaussian mixture modelling similar to established cut-off estimation for CSF biomarkers used for the A and T category[57].

To assess group differences in age and education, one-way ANOVAs with ATN status as between-subject variable were used. Group differences in cognition (MMSE and memory performance) were tested in ANCOVAs with ATN status as between group variable and age, sex and education as covariates. In all cases, post-hoc analysis was performed by two sample t-tests using a Bonferroni correction to account for multiple comparisons. Notably, analyses were restricted to the four groups of the ACH-based progression (1) A-T-N- (2) A+T-N- (3) A+T+N- (4) A+T+N+ since we focused on implications for common AD-related trajectories. The distribution of ATN status per clinical diagnosis was tested by 2-sided Fisher's exact test for distribution differences between cognitively unimpaired (NC, SCD) and cognitively impaired (MCI, DAT) subjects. Significance level is set to $p < .05$ (*) or $p < .001$ (**) respectively.

Testing the evidence for a monotonic decrease of brain volume over ATN progression groups

We aimed to test the evidence of local brain GM volume loss as a process of AD progression. As predicted by the ACH, the volume would decline over the following groups (1) A-T-N- (2) A+T-N- (3) A+T+N-; to (4) A+T+N+. Thus, we hypothesized later ATN stages to be associated with significantly reduced GM in AD-related areas. We estimated a voxel-wise general linear model describing the local GM volume *y* for the 4 given groups as

$$y = X\beta + \epsilon$$

with design matrix *X,* coefficients β and residuals ϵ. The design matrix was chosen to define β_1 as group mean of the first group, and for *g=2,3,4* coefficient β_g as group difference of group *g* and *g-1.* The model was fitted under linear constraints that $\beta_g \leq 0$ for *g=2,3,4* and therefore implementing a monotonic decline of volume across groups *1* to *4* (using MATLAB R2019b's function for constrained optimization lsqlin). For instance if a voxel has a true monotonic decline of volume *y* over groups *1,2,3,4* the model evidence is expected to be higher than for an alternative model with reversed group order e.g. *4,3,2,1*. We further compared different hypothesized and alternative sequences of volume decline progressions using the Bayesian Information Criterion[58] (BIC) which compares the likelihood how well the data is described using a monotonic function while accounting for model complexity (Figure 1).

331 Figure 1: Monotonic and non-monotonic volume decline using ATN.

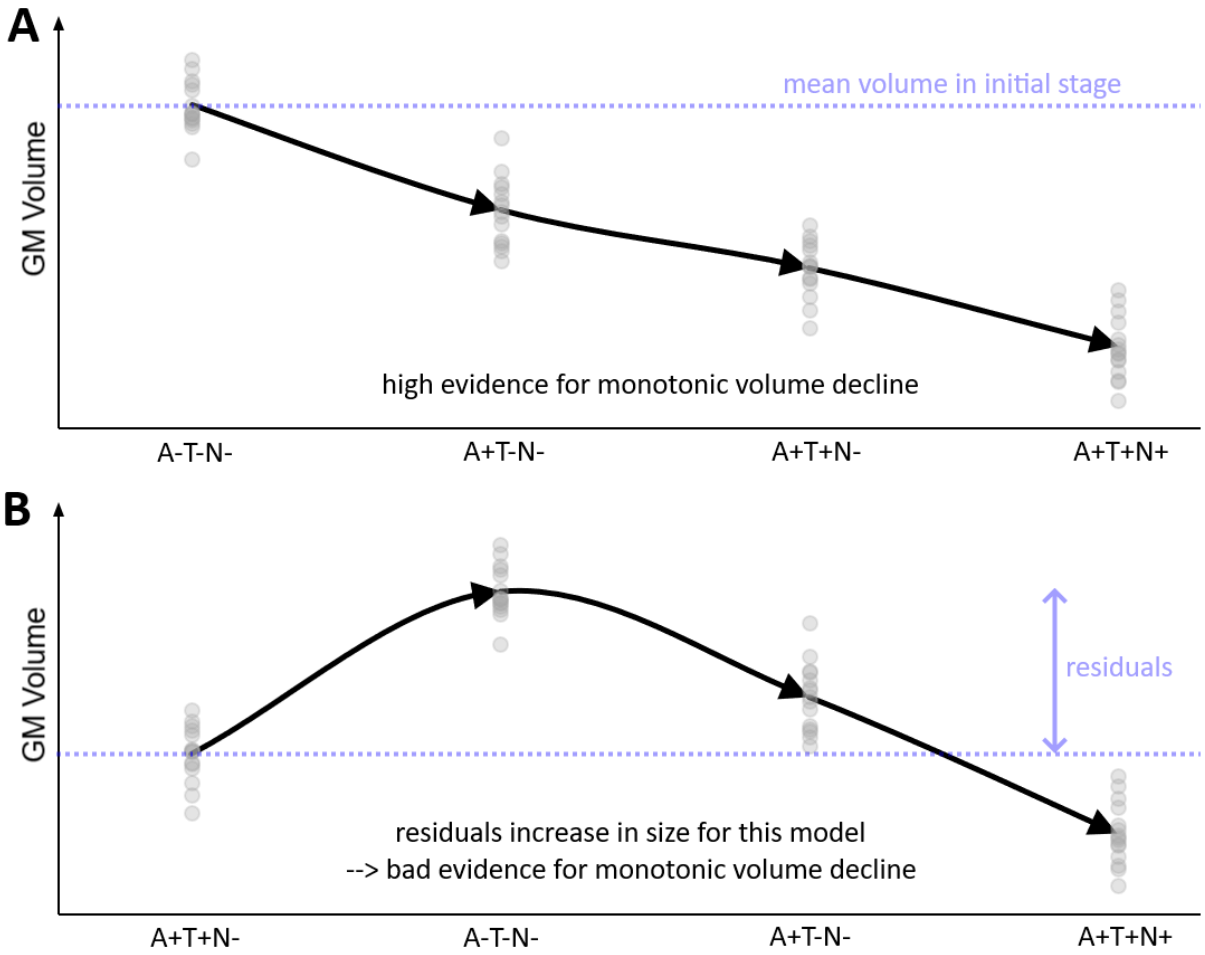

332

333 *A: An illustration of monotonic GM volume decline as hypothesised when following the ACH hypothesis*
334 *using ATN groups. B: A permutated order of the upper case that clearly not shows a monotonic volume*
335 *decline. A temporarily volume increase causes large residuals that cannot be explained by a monotonic*
336 *model. Therefore, the pathway in A would be preferred over B ('higher evidence for monotonic decline in*
337 *A').*

338 First, face validity of the ACH hypothesis was tested by comparing the evidence of the
339 above ACH-based sequence (1) → (2) → (3) → (4) against 23 (=4*3*2*1-1) alternative
340 monotonic progressions generated by permutation which are *a-priori* less plausible if ACH
341 is true. Note that this analysis was restricted to 4 primarily AD-related of all 8 possible
342 ATN classification groups, where it is assumed that Amyloid conversion happens before
343 status conversion of Tau and Neurodegeneration. In a second analysis, the evidence of

the ACH-related volume trajectory was compared against 5 biologically plausible alternative sequences including also ATN groups which are considered outside the AD-continuum, in particular ANT (i.e. Amyloid-conversion first, N-conversion second, Tau-conversion last; therefore 'ANT'), TAN, TNA, NAT, and NTA. These 6 sequences represent all conceivable possibilities to convert in three steps from A-T-N- (no pathology) to A+T+N+ (full pathology).

In this study, all tests were performed both on (A) whole brain voxel-based modulated GM volume images, and (B) a-priori hypothesized ROIs. Voxel-based tests were restricted to GM using an absolute threshold of .05. In addition, the percentage of voxels with the highest evidence for the ACH trajectory inside every ROI mask is provided.

All statistical analyses were performed in MATLAB. Voxel-wise test results are presented as maps with the highest evidence for one particular model and log p maps for inference on statistical parameters such as successive volume decline over groups (using FDR correction for multiple comparisons, $p<0.05$). Finally, the percentage of GM voxels with the highest evidence for a certain progression sequence is provided. All analyses were accounting for covariates age, sex, education, TICV and WHM. All main results are reported for N operationalized by aHV and selected results using CSF Total Tau can be found in the supplementary material.

Results

Sample demographics and ATN group comparisons

Key characteristics of the analysed sample are summarized in Table 1, selected comparisons (Bonferroni) can be found in Figure 2. As expected we found that age

differed across ATN groups ($F(7,429) = 6.65$, $p < .001$). ATN groups showed also differences in years of education ($F(7,429) = 2.63$, $p < .05$). With respect to cognition, we found a significant effect of ATN group ($F(7,426) = 13.46$, $p < .001$), age ($F(1,426) = 14.78$, $p < .001$) and education ($F(1,426) = 19.58$, $p < .001$) on MMSE scoring, but no effect of sex ($F(1,426) = 0.93$, $p = .33$). Similar results were obtained for the memory performance, where ATN status ($F(7,426) = 28.10$, $p < .001$), age ($F(1,426) = 44.54$, $p < .001$), education ($F(1,426) = 39.78$, $p < .001$) and sex ($F(1,426) = 3.87$, $p < .05$) were significant.

Table 1: Sample and ATN group overview.

	A-T-N-	A-T-N+	A-T+N-	A-T+N+	A+T-N-	A+T-N+	A+T+N-	A+T+N+
Group size	143	41	29	14	45	23	61	81
age (years) mean (SD)	69.64 (5.50)	68.10 (5.85)	70.20 (4.56)	70.86 (5.90)	69.97 (5.12)	70.91 (7.10)	73.20 (5.30)	73.46 (5.84)
sex (% female)	48.25%	48.78%	72.41%	28.57%	42.22%	39.13%	47.54%	55.56%
education years mean (SD)	14.65 (2.92)	14.71 (2.87)	13.79 (2.02)	16.57 (2.53)	14.07 (2.53)	14.43 (3.19)	13.67 (3.33)	13.75 (2.98)
MMSE mean (SD)	29.15 (1.19)	28.54 (1.98)	29.14 (1.27)	29.14 (1.61)	29.24 (0.77)	27.52 (3.29)	27.52 (3.06)	26.12 (3.23)
Memory performance mean (SD)	0.39 (0.51)	0.13 (0.84)	0.42 (0.67)	0.01 (0.99)	0.35 (0.64)	-0.52 (1.05)	-0.44 (1.09)	-1.18 (1.00)
CSF Aβ42/40 mean (SD)	0.110 (0.011)	0.108 (0.011)	0.112 (0.013)	0.118 (0.014)	0.074 (0.012)	0.064 (0.015)	0.053 (0.011)	0.050 (0.013)
CSF phospho-Tau (pg/ml) mean (SD)	41.02 (8.81)	39.85 (11.84)	68.02 (10.88)	74.68 (19.41)	41.88 (9.99)	44.49 (9.40)	93.26 (50.38)	95.06 (31.09)
CSF Total Tau (pg/ml) mean (SD)	288.18 (89.16)	291.24 (131.09)	465.98 (115.59)	544.38 (167.71)	321.41 (104.50)	312.96 (94.48)	677.41 (335.83)	778.43 (287.03)
aHV (ml) mean (SD)	3.14 (0.21)	2.64 (0.15)	3.18 (0.24)	2.63 (0.11)	3.12 (0.21)	2.60 (0.21)	3.12 (0.23)	2.56 (0.22)

WMH (ml) mean (SD)	3.29 (5.31)	3.27 (6.07)	1.42 (1.70)	2.09 (2.83)	3.19 (3.61)	4.66 (6.05)	6.99 (11.61)	6.34 (7.96)

Overview on test sample and ATN group statistics. aHV: adjusted hippocampal volume; WMH: white matter hyperintensities.

As shown in Figure 2, the age increased while global cognition (MMSE) and memory performance decreased following a hypothesized disease progression using the ACH sequence (A-T-N- → A+T-N- → A+T+N- → A+T+N+). No systematic pattern was found for years of education. These effects could be reproduced using CSF Total Tau for N (Supplemental File 1).

Figure 2: Comparison between selected ATN groups.

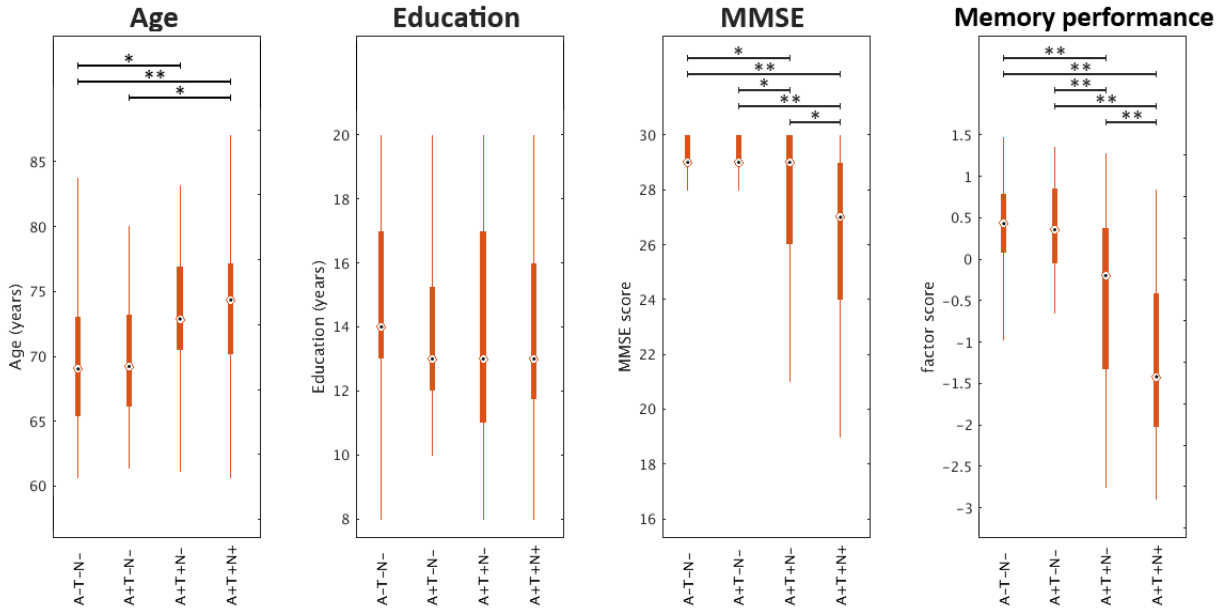

*Boxplots of age, sex, cognition for selected ATN groups. *: p < .05 after Bonferroni correction, **: p < .001 after Bonferroni correction.*

Association of ATN status and clinical diagnosis

We observed an association of the ATN status and clinical diagnosis groups comparing cognitively unimpaired (NC, SCD) and cognitively impaired (MCI, DAT) participants for A-T-N- ($p < .001$), A-T+N- ($p < .05$), A+T-N- ($p < .05$), A+T+N- ($p < .05$) and A+T+N+ ($p <$

.001). No non-random association was found for A-T-N+ (p = .49), A-T+N+ (p = .40) and A+T-N+ (p = .26). Compared to A-T-N-, the highest relative risk for DAT was found in A+T+N+ (30.90 times higher) and A+T-N+ (15.54 times). The lowest risk for DAT relative to A-T-N- was in A-T+N- (2.47 times higher), while no DAT cases were recorded in A-T+N+ or A+T-N-. Results suggested that more impaired clinical groups, especially DAT, were found more often among the Alzheimer's continuum ATN groups (i.e. in A+), while cognitively unimpaired status was rather associated to no brain pathology (i.e. A-T-N-). For percentual distribution see Figure 3. A similar pattern was observed for N measured by CSF Total Tau (Supplemental File 2).

Figure 3: Distribution of ATN status and clinical diagnosis.

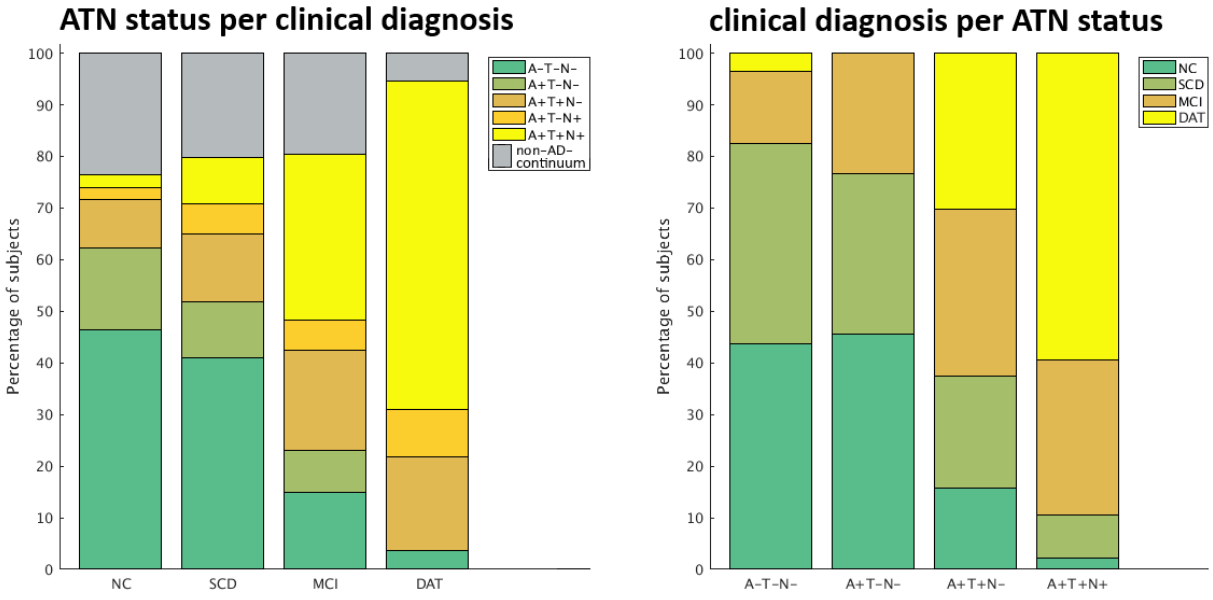

Left: percentual distribution of selected ATN groups per clinical diagnosis; right: percentual distribution of clinical diagnosis per ATN groups.

Assessing face validity of the ACH hypothesis using local brain volume

As a next goal, we identified brain regions where volume progression across ATN groups is compatible with the ACH hypothesis. More specifically, if the ACH is true it might be expected to observe a monotonic decline of volume over groups A-T-N- → A+T-N- →

A+T+N- → A+T+N+ in the hippocampal network[25]. The regions showing significant GM volume decline over this ACH sequence (of ATN biomarker conversions) are illustrated in Figure 4A (log p map, $p < .05$ FDR-corrected, N based on hippocampal volume, accounting for covariates age, sex, education, TICV and WMH). Strongest effects are found in the MTL region (peak: left post. hipp. x = -28, y = -22, z = -19, log p = 86.70). Further regions with significant GM volume loss following the ACH sequence are the orbital and basal forebrain, large parts of the temporal lobe, the insular cortex, the basal ganglia, the cingulate gyrus, the precuneus, (medial) premotor regions and the parietal and occipital lobes. When using CSF total Tau instead of hippocampal volume for operationalization of the 'N' category, we observed consistent but slightly less widespread shrinkage of local GM (peak: left ant. hipp. peak x = -26, y = -10, z = -17, log p = 21.41, Figure 4B).

Figure 4: Volume decline following the ACH sequence.

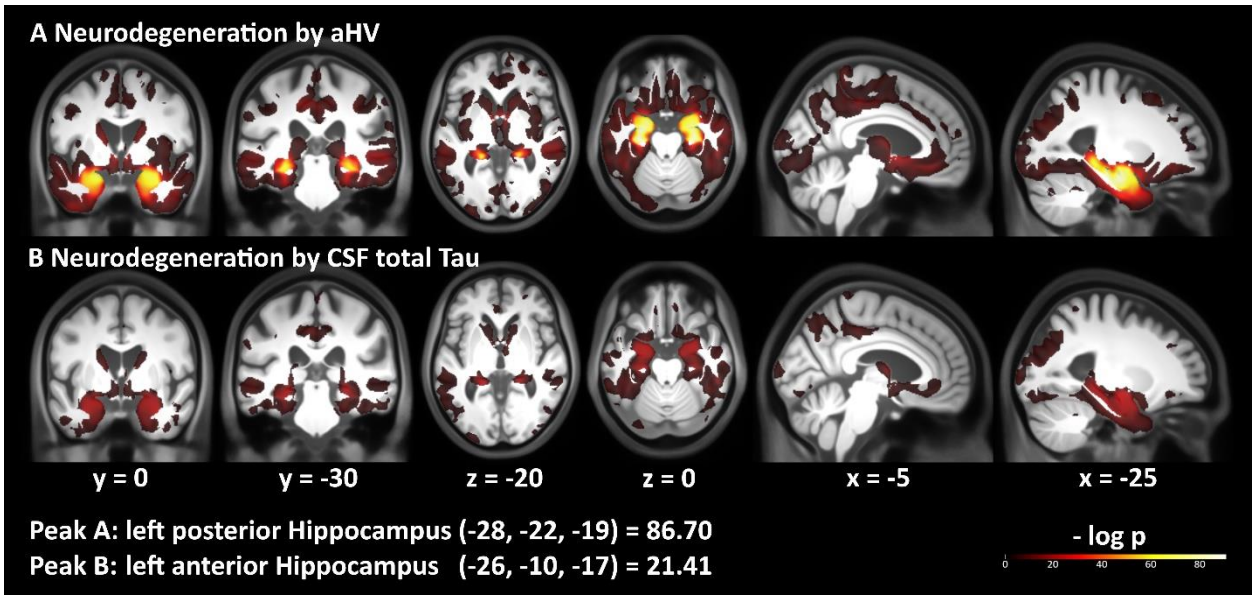

Regions showing significant GM volume loss along the ACH sequence. Unmasked log p map with $p < .05$, FDR-corrected. A: Neurodegeneration (N) defined by aHV; B: Neurodegeneration (N) defined by CSF total Tau.

It is important to note that testing for 'any' local volume decline over groups that align with the ACH-related progression might still reveal brain areas where alternative disease progressions are even more likely. Therefore, in an explorative analysis we compared voxel-wise evidence of the hypothesized ACH progression (or model) against 23 biologically less plausible (permuted) conversion sequences among the ATN classification groups associated with the AD continuum e.g. the above stated group progression but in reversed order. First, we applied a voxel-based test of monotonic GM volume decline using the Bayesian Information Criterion. Figure 5a illustrates the resulting regions with highest evidence for three selected progressions. Since only one sequence of diagnostic conversions can have the highest evidence in a given brain region (when compared to other progressions), these maps revealed non-overlapping areas of the brain. For 8.99% of all explored GM brain regions, ACH was indeed found to be the most evident progression sequence showing monotonic volume decline (Figure 5b). This especially involved the anterior MTL, hippocampus, parahippocampal gyrus and fusiform gyrus while the general pattern of regions most compatible with ACH is similar to the above presented findings.

448 Figure 5: Face validity of ACH using VBM.

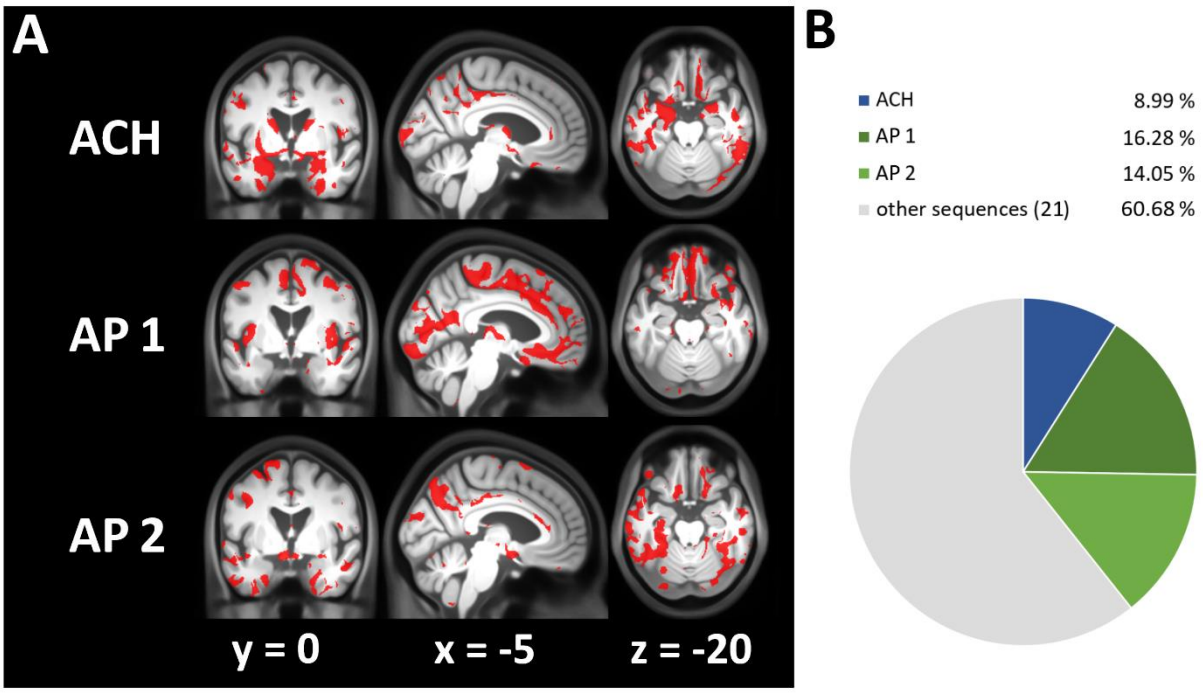

449

450 *Voxel-based evidence for monotonic volume decline over 24 sequences gained by permutation of the ACH*
451 *sequence (ACH, A-T-N-→A+T-N-→A+T+N-→A+T+N+); AP 1: A+T-N-→A+T+N-→A-T-N-→A+T+N+; AP 2:*
452 *A+T-N-→A-T-N-→A+T+N-→A+T+N+; A: voxels where sequence shows highest evidence; B: percentage*
453 *of gray matter voxels where sequence has highest evidence.*

454 However, this analysis also suggested that the ACH sequence was not the most evident
455 progression (among 24 tested) in frontal lobe, insular cortex, precentral and postcentral
456 gyri or the cerebellum. Our analysis revealed several brain regions in which alternative
457 sequences over ATN groups were better reflective of monotonic volumetric decline. More
458 specifically, alternative progressions AP 1 (A+T-N-→A+T+N-→A-T-N-→A+T+N+) and AP
459 2 (A+T-N-→A-T-N-→A+T+N-→A+T+N+) showed highest evidence in 16.28% and
460 14.05% of the GM respectively (Figure 5). Interestingly, both assume a transient volume
461 increase when transitioning to Amyloid-positivity (i.e. GM volume of A+T-N- > A-T-N-)
462 followed by the lowest GM volume in A+T+N+. AP 1 was the conversion sequence having
463 highest evidence in cortical regions (especially frontal lobe, orbital frontal, premotor

regions, insular cortex). AP 2 showed highest evidence in parts of the posterior MTL, the middle and posterior cingulate gyrus, and cortical clusters (the precuneus, temporal, parietooccipital lobe).

Table 2 shows the results for a similar but complementary ROI-level analysis of monotonic GM decline in amygdala, hippocampus, entorhinal cortex and precuneus defined using an MRI atlas. The ACH-based progression was found to be the best fitting sequence to describe monotonic GM volume loss in amygdala and entorhinal cortex. For all ROIs, the ACH progression was found to be among top 5 most likely sequences (out of 24). Surprisingly, AP 1 showed highest evidence for hippocampal ROI volume loss, while the precuneus volume was best described by AP 2. One potential disadvantage of the definition of the 'N' category is the dependence on atlas-based ROIs, e.g. for the hippocampus. When using CSF Total Tau for definition of the 'N' category, the ACH sequence was also found to optimally describe monotonic GM loss especially in the MTL. On ROI level the ACH sequence was always the most or second most evident pathway (out of 24; Supplemental File 3&4).

Table 2: Face validity of ACH in selected ROIs.

Region	Sequence with highest evidence	T	P	ACH on rank nr. (of 24)	ACH VX%
AMG	ACH	-13.69	2.53e-34	1	80.99
Hippocampus	AP 1	-14.88	6.76e-39	5	26.27
Entorhinal Cortex	ACH	-7.30	1.13e-12	1	48.46
Precuneus	AP 2	-3.90	5.76e-05	4	13.78
Braak I/II	ACH	-16.11	1.15e-43	1	25.13
Braak III/IV	Other1	-6.97	8.59e-12	5	17.97
Braak V/VI	Other1	5.06	3.54e-07	5	7.31

ROI based testing for monotonic volume decline over 24 sequences gained by permutation of the ACH sequence. Braak stage volumes are aggregated Freesurfer ROI volumes. ACH: A-T-N-→A+T-N-→A+T+N-→A+T+N+; AP 1: A+T-N-→A+T+N-→A-T-N-→A+T+N+; AP 2: A+T-N-→A-T-N-→A+T+N-→A+T+N+;

Other1: A+T+N- → A+T-N- → A-T-N- → A+T+N+. ACH VX%: Percentage of voxels with highest evidence for ACH sequence inside the ROI mask.

Comparing progression sequences towards AD pathology including non-AD continuum groups

All above comparisons were focused on only four ATN groups from the AD continuum (A-T-N-, A+T-N-, A+T+N-, A+T+N+). However, these AD continuum-related groups do not enable direct comparisons of ACH-implied conversion sequences against an alternative timing of events such as Tau positivity preceding Amyloid positivity (e.g. A-T+N+ converting to A+T+N+). We therefore compared the ACH-based sequence to five other biologically possible conversion schemes from A-T-N- towards A+T+N+ (denoted as ANT, TAN, TNA, NAT, NTA). For this comparison the conversion sequences are denoted in the order of each biomarker becoming positive, e.g., TAN stands for: Tau category becomes positive first, Amyloid second, Neurodegeneration last (A-T-N- → A-T+N- → A+T+N- → A+T+N+). Again, Bayesian Information Criterion (BIC) was used to identify conversion sequences with highest evidence for monotonic volume decline both on a voxel as well as ROI-level.

Brain regions with highest evidence for above progressions are characterized in Figure 6. According to our analysis A-first sequences (ACH/ATN, ANT), T-first sequences (TAN, TNA) and N-first sequences (NAT, NTA) showed the highest evidence for monotonic volume decline in 64%, 35% and 0.01% of GM respectively. Local GM regions with highest likelihood for ACH were especially found in the MTL (with an exception of the right anterior hippocampus and parahippocampal gyrus), but also in the basal ganglia (caudate ncl., putamen, thalamus) and precuneus. More supporting clusters for ACH/ATN were observed in all cortical lobes making it clearly the most likely sequence in large parts of GM in this comparison. The ANT progression showed highest evidence in complementary

regions of the MTL not covered by ACH/ATN (see above) with additional regions in the basal ganglia (ncl. accumbens), medial frontal lobe, the insular cortex and premotor regions. T-first sequences were most likely only in the cerebellum and some cortical regions including the medial occipital lobe. All of these four sequences showed evidence for different parts of the cingulate gyrus. N-first sequences were only seen in very minor portions of the GM.

Figure 6: Comparing progression sequences towards AD pathology using VBM.

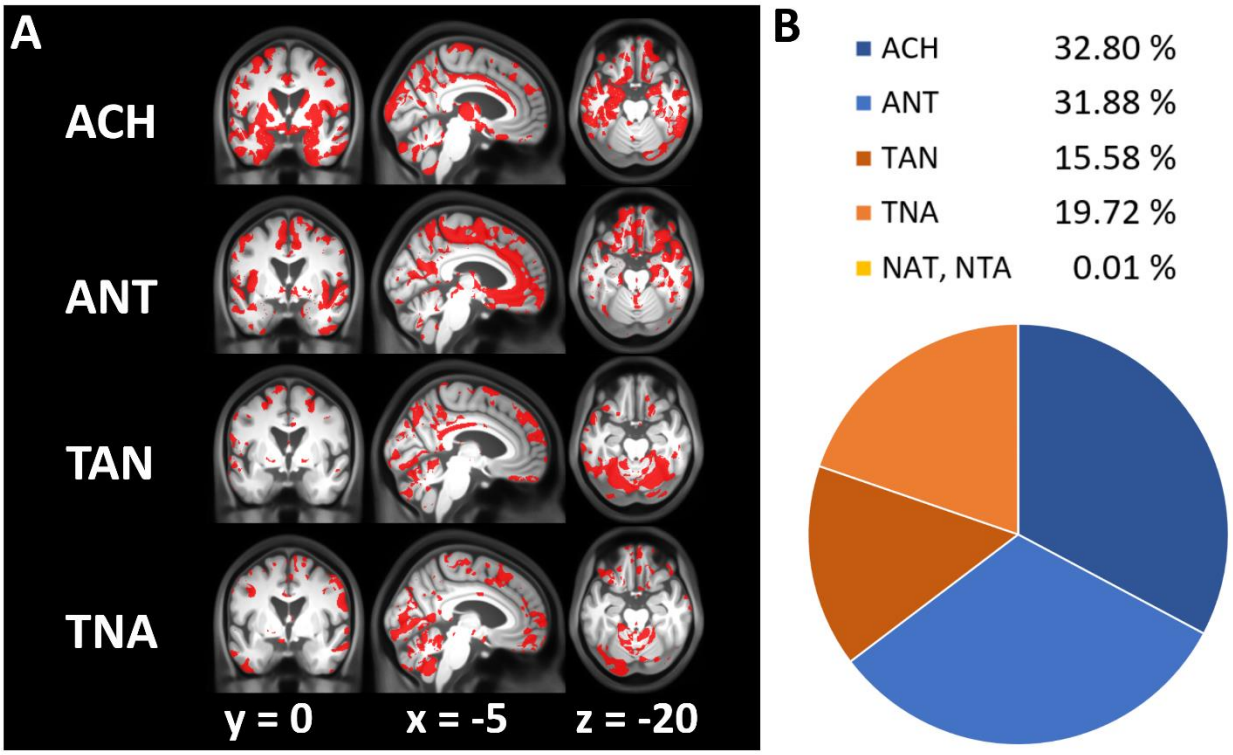

Regions with highest evidence for monotonic volume decline assuming 6 potential disease progressions from A-T-N- towards A+T+N+ (ACH, ANT, TAN, TNA, NAT, NTA). Sequences are denoted in the order of biomarker positivity along the pathway (e.g. ANT = Amyloid-positivity first, Neurodegeneration second, Tau last). A: voxels where sequence shows highest evidence; Notably, regions of highest evidence for each progression are disjunct. B: percentage of gray matter voxels where sequence has highest evidence. N-first sequences (NAT, NTA) are not shown as only few voxels are supported.

In the complementary ROI analysis, conversion sequences with monotonic volume decline were compared for same ROIs as above. The most evident sequences for volume

loss per ROI and matching effect size are presented in Table 3. Interestingly, ACH/ATN was the most evident progression for amygdala, entorhinal cortex and precuneus. In hippocampus however, the ANT progression was found to show the highest evidence for the data. Our analysis revealed no indications for the superiority of T-first or N-first over A-first sequences in these ROIs. Notably, above findings were mainly reproduced using CSF Total Tau as neurodegeneration marker. Here, ACH was also the most prominent sequence: On voxel-level, more than 41% of GM showed highest evidence for the ACH sequence (Supplemental File 5). On ROI-level, ACH was the most evident sequence with exception of amygdala and entorhinal cortex, where TAN was more likely which is in contrast to the results of aHV-based Neurodegeneration (Supplemental File 6).

Table 3: Comparing progression sequences towards AD pathology including non-AD continuum groups in selected ROIs.

Region	Best sequence	T	P	ACH on rank nr. (of 6)	ACH VX%
AMG	ACH	-12.93	8.22e-33	1	89.62
Hippocampus	ANT	-18.07	5.74e-55	2	58.18
Entorhinal Cortex	ACH	-7.25	9.78e-13	1	89.05
Precuneus	ACH	-3.93	4.86e-05	1	30.92
Braak I/II	ACH	-16.20	1.07e-46	1	57.95
Braak III/IV	ANT	-7.67	5.64e-14	2	46.02
Braak V/VI	ANT	-4.21	1.53e-05	2	28.60

ROI based testing for monotonic volume decline over 6 possible sequences from A-T-N- towards A+T+N+ (ACH, ANT, TAN, TNA, NAT, NTA). Braak stage volumes are aggregated Freesurfer volumes of regions that mirror Braak stages. ACH VX%: Percentage of voxels with highest evidence for ACH sequence inside the ROI mask.

Concordance of Braak stage trajectory and the ACH trajectory

In addition to above reported ROIs, the two voxel-based analyses of compatibility of the ACH sequence with monotonic GM volume decline were aggregated for larger Braak

stage composite regions (Table 2 & 3). Here, stage I/II encompasses the hippocampus and entorhinal cortex, stage III/IV the limbic regions and stage V/VI the remaining cortical regions like precuneus or primary sensory/motor regions. We asked, how much of GM at some stage showed highest evidence for ACH. On voxel-level, the percentage of voxels with highest evidence for the ACH sequence decreased from 25.1% in stage I/II to 7.3% in stage V/VI for the first comparison (face validity of ACH). For the second comparison (including non-AD continuum groups) there was also a noticeable decrease of ACH compatible GM voxels from 58.0% in stage I/II to 28.6% in stage V/VI (see Table 2 & 3).

Thus, on ROI-level, ACH-related ATN sequence across groups was the most evident conversion sequence which is compatible with a monotonic volume decline in Braak stage I/II. For ROIs reflecting stages III/IV and V/VI, ACH was under the most evident 5 (of 24) respectively 2 (of 6) sequences and thus not the most likely explanation for decline anymore. Test statistics and p-values were decreasing with higher Braak stages (stage I/II & III/IV: $p < .001$; V/VI: $p < .05$) which supports that ACH compatibility reduces with Braak stage. Using CSF Total Tau instead of hippocampal volume, a similar trend was observed while more voxels supported ACH in stage I/II (stage I/II & III/IV: $p < .001$; V/VI: $p > .05$), Supplemental File 3&6).

Discussion

Since the ATN classification was postulated in 2016[24], several studies compared ATN groups to a traditional clinical dementia classification[26,27,59,30,29,60,61]. However, a discussion of ATN in context of biological or structural brain changes during AD including local (e.g. voxel-based) brain morphology and the Amyloid Cascade Hypothesis (ACH)

566 can be found to a much lesser extent in previous research[31-33]. This study aimed to focus
567 on these neglected aspects of interest.

568 Our comparison between ATN status and clinical diagnosis suggested advanced clinical
569 diagnostic status with increasing pathology levels following the ACH group conversion
570 sequence. This is consistent with earlier work[27,59,30] where a similar pattern has been
571 observed. The A+T+N+ group has previously been reported to show the highest
572 conversion rate to DAT and an increased risk for cognitive decline[26,27,29,60,30,61]. In line
573 with these findings our results suggested substantial memory performance reductions in
574 later ATN stages.

575 Using MRI and voxel-based morphometry (VBM) we first tested the face validity of a
576 monotonic GM volume decline over the 4 ATN stages (1) A-T-N- (2) A+T-N- (3) A+T+N-
577 (4) A+T+N+ as implied by the ACH and previous work suggesting GM volume loss during
578 ACH progression in clinical DAT. In contrast to previous with strong prior assumptions
579 about ROIs, our emphasize here was on reporting also complementary voxel-based
580 results. More specifically, in line with previous findings brain regions following monotonic
581 volume decline over ATN stages (1)-(4) involved the hippocampus[62,17,46,45,63-68],
582 amygdala[62,17,46,45,65,67,68], temporal gyri[17,46,64,66,67], thalamus[62,17,65,63], precuneus[62,17,64,66]
583 and cingulate gyrus[62,17,63,64,66,69]. Consistent with some previous work[69,63,66] a decline in
584 parts of the cingulate gyrus and insula were observed in our study. Regions that are
585 expected to be affected in very late AD such as frontal[17,66] and occipital[64,45,63,66] lobes or
586 less affected such as those around central sulcus[46,64,66] showed only minor effects in
587 terms of a monotonic decline over ATN stages (1)-(4).

588 Notably the ACH is still part of an ongoing discussion as anti-amyloid treatments showed
589 only limited success[70,71]. Furthermore, the causal link between Amyloid, Tau and resulting

neurodegeneration and dementia is a challenging research topic[19,20] which might be mediated by alterations in neuropil[71], synapses[72] or functional connectivity[73]. Our study revealed strong evidence for an ACH-related monotonic atrophy pattern both on voxel-level but also on ROI-level especially focussed on typical AD-related regions such as the MTL. However, we also observed many gray matter areas where a monotonic volume trajectory along the ACH-implied group progression sequence did show the highest evidence. We identified alternative progressions (denoted AP 1 and AP 2) indicating that there are several cortical regions where the GM volume was found to be higher in the A+T-N- group than in A-T-N-. These were mainly found in cortical regions which are often less strongly affected by AD[66,17]. One might speculate that either Amyloid deposition related tissue expansion[74,75] and/or sampling effects due to individual differences of brain reserve[76] might alter brain volume patterns across ATN groups and the progression along the ACH trajectory. A biphasic model of neurodegeneration has been previously suggested by Fortea et al.[74] hypothesizing that cortical thickening might occur when Aβ becomes abnormal, which presumably reflects inflammation-related swelling, followed by thinning once tau pathology emerges. The authors found Amyloid-related thickness increases in middle temporal, inferior and superior parietal, occipital regions and precuneus which is similar to our findings. Another recent publication also observed Amyloid-related regional volume increase in A+T-N- for the basal forebrain, postcentral gyrus, middle occipital gyrus, and putamen when comparing to A-T-N-[77]. As described above, large parts of the cingulate gyrus did suggest a monotonic volume decline along ACH group progression. However, ACH did not necessarily reveal the highest evidence in the entire cingulate as there were also portions with highest evidence for non-monotonic volume decline (subcallosal to middle cingulate in AP1 & middle to posterior

cingulate in AP2). This renders the cingulate a potential candidate region for brain reserve or biphasic model that requires further research.

Under the assumption that patients will convert from negative to positive ATN biomarkers, six patterns of conversions are possible when non-AD pathology ATN groups are additionally included. When testing for monotonic volume decline across these patterns, the highest evidence was found for sequences where Amyloid converts before either Tau or Neurodegeneration (e.g. ATN, ANT), and this was observed in 65% of all gray matter brain areas, especially in AD-related regions. We were able to replicate our finding using ROI-based analyses. In contrast, conversion patterns where Tau converted before Amyloid (TAN, TNA) showed highest evidence for a monotonic volume decline in cortical regions that are atypical for AD pathology. Support for our findings comes from a longitudinal study of 262 non-demented elderly to monitor ATN biomarker progress[32]. It was found that ACH was the most common path of biomarker conversion, but also ANT, TAN and NAT occurred. In contrast, we observed no evidence for NAT in terms of GM volume decreases. It is worth mentioning that per definition, A-T+ or A-N+ groups are not part of the AD-continuum, these groups might initially point to other diseases like primary tauopathies, hippocampal sclerosis/TDP-43 or ischaemic diseases[24]. As remarked by [1] and [32], the occurrence of conversion sequences other than ACH in real world data might be explained (a) by coincidence of AD- and non-AD pathologic changes (e.g. in A+T-N+) or (b) long-time subthreshold biomarker trends matching the ACH that are not recognized due to a binary classification with disadvantageous thresholds[1,32]. Another study provides more support for our hypothesis of an ACH-related temporal order of biomarker progress by monitoring between-group biomarker changes in an longitudinal approach using the ATN classification[31].

638 Furthermore, our morphometric study revealed evidence to support the consistency
639 between the ACH and Braak staging. Brain regions that are expected to be earlier
640 affected by AD-pathology-linked tau deposition (stage I-IV, MTL, limbic system) showed
641 stronger evidence for monotonic GM volume decline over a sequence of conversions than
642 later stages (stage V/VI, cortical regions). As it is already known that brain atrophy often
643 follows Tau and NFT aggregation[65], both hypotheses were not mutually exclusive. In our
644 analysis, the stronger evidence for volume decline in the amygdala was surprising when
645 comparing to the hippocampus. As [78] remarked, Tau pathology in the amygdala is already
646 beginning with Braak stage I/II. However, this effect was not reproducible with
647 Neurodegeneration by CSF Total Tau.

648 It is known that alternative choices of markers for the N category may have a strong
649 impact on ATN status assignment and longitudinal prediction of cognition[79,80]. The large
650 pool of possible classification methods limits intercomparability between ATN studies
651 dramatically. In our large study, both variants of ATN classification approaches showed
652 converging evidence for the ACH hypothesis. We were not able to determine a superior
653 combination, as both tested N markers have advantages and caveats. The usage of aHV
654 leads to overall stronger effect sizes but one might argue that there is a circularity in
655 defining ATN groups using volumetry and analyzing ATN-related local brain
656 morphometry. Neurodegeneration defined by aHV is a discrete marker of general
657 neuronal loss and the group assignment was carried out using a ROI-rather than voxel-
658 based approach. GM volume (as analyzed by VBM) on the other hand allows a
659 continuous whole brain local analysis on voxel-level and does not align with N for most
660 brain regions.

661 Although VBM revealed the highest evidence for ACH-related monotonic volume decline
662 in the hippocampus, regions in cortical areas showed compatible monotonic

progressions. Taking advantage of the voxel-based approach, differences between sequences could be identified even inside the hippocampus (ACH supports anterior Hippocampus, AP2 posterior hippocampus). It is worth mentioning that the approach is not limited to VBM measurements, in contrast to developmental and plasticity studies stronger expectations for monotonic trajectories do exist for brain volumes in aging and AD. Alternative N categories (such as CSF Total Tau) might also have limitations. The combination of CSF phospho-Tau (T category) and CSF Total Tau (N category) is used in some studies[26,60,61], while a strong correlation between both markers strongly underrepresents some ATN groups (A?T+N-, A?T-N+). In a recent publication[28] it was possible to replace CSF Total Tau by CSF phospho-Tau without significant impact on the model. Although there is only a weak correlation between aHV and CSF Total Tau as N markers in our study, a similar pattern of local GM volume decline was revealed. This further suggests that a morphometrical analysis with aHV is applicable.

Limitations

This study has several methodological limitations. The first challenge was the hippocampal cut-off estimation: The large sample size does not allow to perform atrophy reference methods like autopsy or visual rating of FDG-PET or MRI. Thus, no estimation of sensitivity or specificity was possible, which prohibits a ROC analysis and Youden's index. Although aHV has a clear unimodal gaussian distribution, it is possible to perform a Gaussian mixture modelling to separate between normal and decreased volumes. A similar approach was performed by[77]. As our data is cross-sectional, no real progression over disease progression and conversions can be modelled and tested. We compensated potential influences of covariates by correcting for demographic marker such as age, sex and education, vascular damage and intracranial volume. This improves comparability (matching) across different ATN groups and increases validity of the underlying cross-

sectional progression. Once available, longitudinal DELCODE follow-up data will be used for further validation.

Conclusion

Early Amyloid status conversion (before Tau and Neurodegeneration) aligns with pattern of brain volume loss observed during AD progression. The ATN classification and the Amyloid cascade hypothesis are compatible with a monotonic progression of MTL atrophy but using the ATN classification system for staging our study revealed indications for non-monotonic progressions in other areas such as several cortical fields.

709 # Glossary

ACH	Amyloid Cascade Hypothesis
AD	Alzheimer's disease
DAT	Dementia of Alzheimer’s type
aHV	Adjusted hippocampal volume
AN(C)OVA	Analysis of (co-) variance
ATN	Classification based on Amyloid / Tau / Neurodegeneration pathology
BIC	Bayesian Information Criterion
CAT	Computational Anatomy Toolbox
CDR	Clinical Dementia Rating
CERAD	Consortium to establish a registry for Alzheimer's disease
NC	Non-complaining healthy control
CSF	Cerebrospinal fluid
FDR	False Discovery Rate
FLAIR	Fluid attenuated inversion recovery
GM	Gray matter
MCI	Mild Cognitive Impairment
MMSE	Mini-mental state examination
MPRAGE	Magnetization prepared rapid gradient echo

MRI	Magnetic resonance imaging
MTL	Medial temporal lobe
NFT	Neurofibrillary tangles
ROI	Region of interest
SCD	Subjective Cognitive Decline
SPM	Statistical Parametric Mapping
TICV	Total intracranial volume
VBM	Voxel-based Morphometry
WM	White matter
WMH	White matter hyperintensities

Declarations

Ethics approval and consent to participate

DELCODE is retrospectively registered at the German Clinical Trials Register (DRKS00007966), (04/05/2015) and was approved by ethical committees and local review boards. All participants gave written informed consent to participate.

Consent for publication

Not applicable

Availability of Data and Materials

The code used during the current study are available from the corresponding author on reasonable request. Data, study protocol and biomaterials can be shared with partners based on individual data- and biomaterial transfer agreements. Requests can be addressed to the DELCODE steering committee.

Competing Interests

The authors declare that they have no competing interests.

Funding

The study was funded by the German Center for Neurodegenerative Diseases (Deutsches Zentrum für Neurodegenerative Erkrankungen (DZNE)), reference number BN012.

Author's contributions

The study was designed by E.D., M.W., A.S. and F.J. Data analysis was performed by N.H. N.H., G.Z., and E.D. wrote the manuscript. All authors reviewed the paper.

741 ## Acknowledgements

742 Not applicable

743

744

745

746

747

748

749

750

751

752

753

754

755

756

757

758

759

760

Supplement

Supplemental File 1: Comparison between selected ATN groups using CSF-total-Tau.

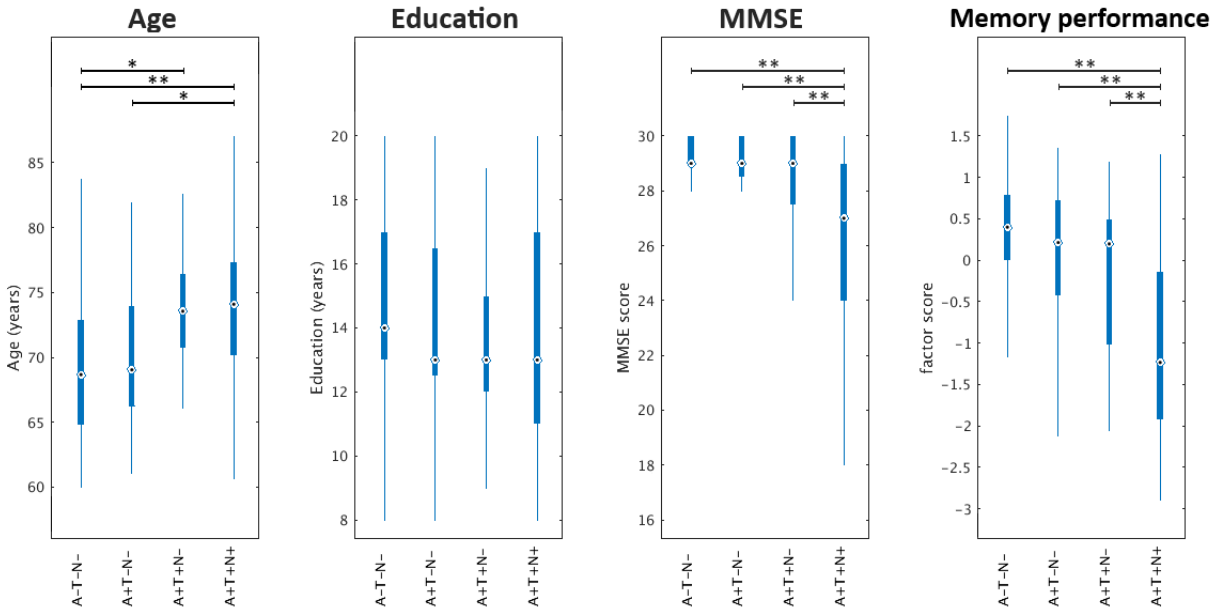

*Boxplots of age, sex, cognition for selected ATN groups. *: p < .05 after Bonferroni correction, **: p < .001 after Bonferroni correction. Neurodegeneration (N) by CSF Total Tau.*

Supplemental File 2: Distribution of ATN status and clinical diagnosis using CSF-total-Tau.

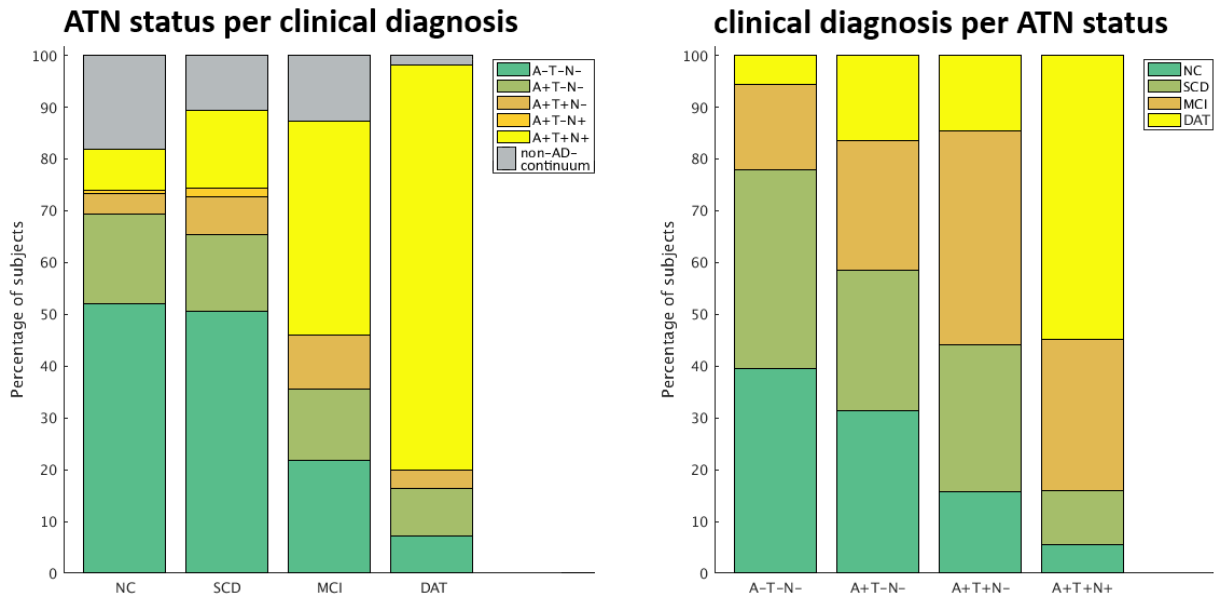

Left: percentual distribution of selected ATN groups per clinical diagnosis; right: percentual distribution of clinical diagnosis per ATN groups. Neurodegeneration (N) by CSF Total Tau.

Supplemental File 3: Face validity of ACH using selected ROIs and CSF-total-Tau.

Region	Best sequence	T	P	ACH on rank nr. (of 24)	ACH VX%
AMG	Other2	-7.10	3.17e-12	2	14.42
Hippocampus	ACH	-6.20	7.34e-10	1	47.86
Entorhinal Cortex	Other2	-4.71	1.73e-06	2	43.94
Precuneus	Other3	-2.35	.0095	2	18.00
Braak I/II	ACH	-6.65	5.10e-11	1	50.38
Braak III/IV	Other2	-4.52	4.16e-06	2	16.58
Braak V/VI	Other2	-1.64	.0513	2	5.52

ROI based testing for monotonic volume decline over 24 sequences gained by permutation of the ACH sequence. Braak stage volumes are aggregated Freesurfer ROI volumes. Other2: A-T-N- → A+T+N- → A+T-N- → A+T+N+; Other3: A+T-N- → A-T-N- → A+T+N- → A+T+N+. ACH VX%: Percentage of voxels with highest evidence for ACH sequence inside the ROI mask. Neurodegeneration (N) by CSF Total Tau.

806 Supplemental File 4: Face validity of ACH using VBM and CSF-total-Tau.

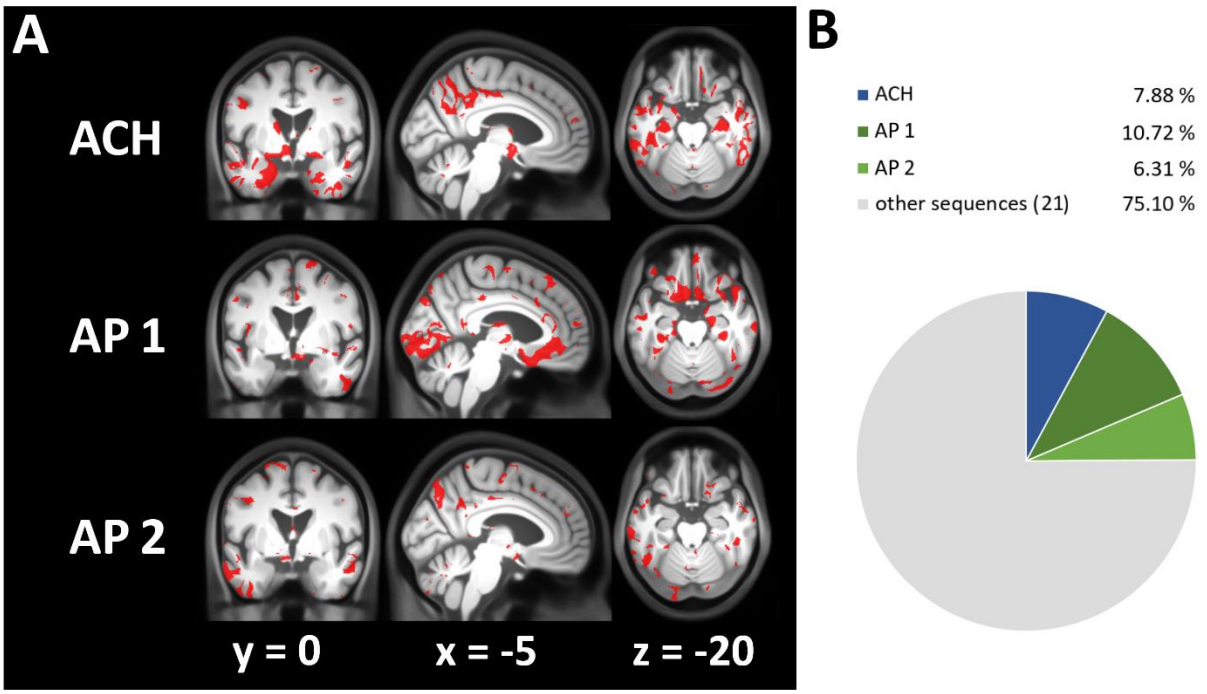

807

808 *Voxel-based evidence for monotonic volume decline over 24 sequences gained by permutation of the ACH*
809 *sequence (ACH, A-T-N-→A+T-N-→A+T+N-→A+T+N+); AP 1: A+T-N-→A+T+N-→A-T-N-→A+T+N+; AP 2:*
810 *A+T-N-→A-T-N-→A+T+N-→A+T+N+; A: voxels where sequence shows highest evidence; B: percentage*
811 *of gray matter voxels where sequence has highest evidence. Neurodegeneration (N) by CSF Total Tau.*

812

813

814

815

816

817

818

819

820

821 Supplemental File 5: Comparing progression sequences towards AD pathology using

822 VBM and CSF-total-Tau.

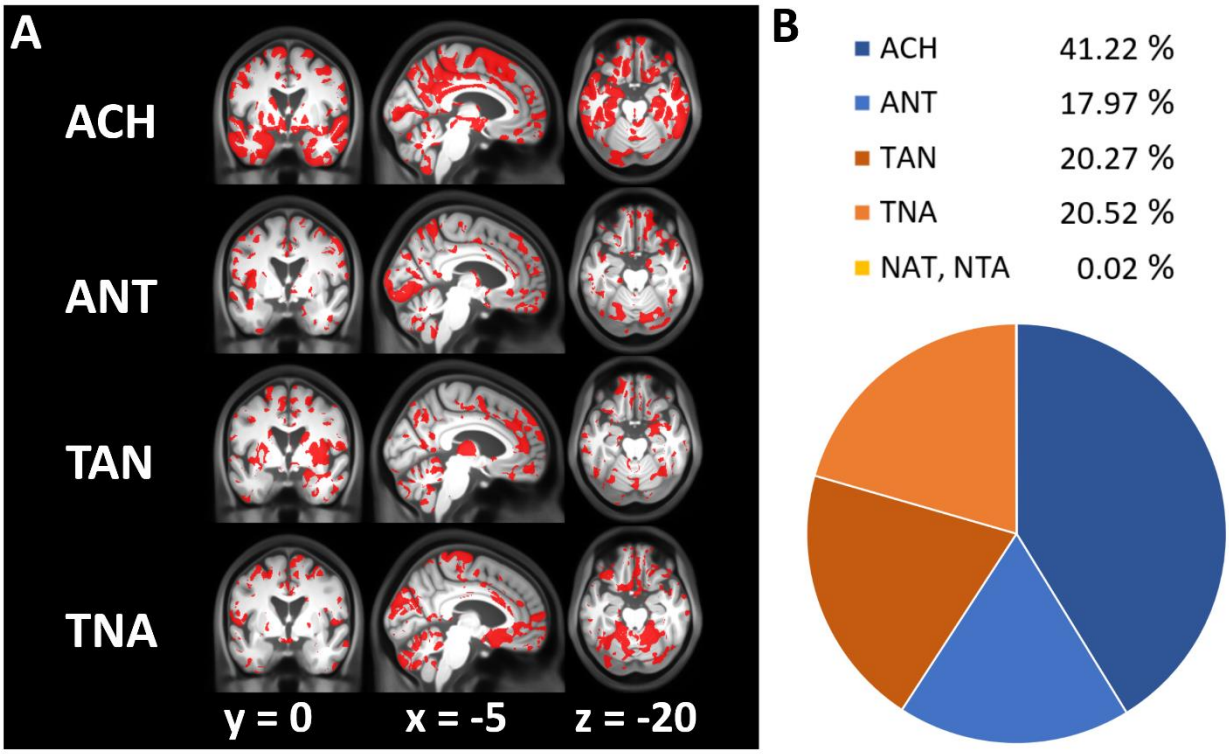

823

824 *Voxel-based evidence for monotonic volume decline over 6 possible sequences from A-T-N- towards*
825 *A+T+N+ (ACH, ANT, TAN, TNA, NAT, NTA). Sequences are denoted in the order of biomarker positivity*
826 *along the pathway (e.g. ANT = Amyloid-positivity first, Neurodegeneration second, Tau last). A: voxels*
827 *where sequence shows highest evidence; B: percentage of gray matter voxels where sequence has highest*
828 *evidence. N-first sequences (NAT, NTA) are not shown as only few voxels are supported.*
829 *Neurodegeneration (N) by CSF Total Tau.*

830

831

832

833

834

Supplemental File 6: Comparing progression sequences towards AD pathology using selected ROIs and CSF-total-Tau.

Region	Best sequence	T	P	ACH on rank nr. (of 6)	ACH VX%
AMG	TAN	-6.83	1.48e-11	5	49.06
Hippocampus	ACH	-6.13	9.81e-10	1	75.41
Entorhinal Cortex	TAN	-4.67	2.06e-06	2	72.55
Precuneus	ACH	-2.85	.0023	1	54.50
Braak I/II	ACH	-6.53	9.41e-11	1	76.52
Braak III/IV	ACH	-4.34	8.72e-06	1	50.96
Braak V/VI	ACH	-1.60	.0557	1	39.84

ROI based testing for monotonic volume decline over 6 possible sequences from A-T-N- towards A+T+N+ (ACH, ANT, TAN, TNA, NAT, NTA) including also non-AD continuum groups. Braak stage volumes are aggregated Freesurfer ROI volumes. ACH VX%: Percentage of voxels with highest evidence for ACH sequence inside the ROI mask. Neurodegeneration (N) by CSF Total Tau.

References

1. Jack CR, Knopman DS, Jagust WJ, et al. Tracking pathophysiological processes in Alzheimer's disease: an updated hypothetical model of dynamic biomarkers. *The Lancet Neurology*. 2013;12(2):207-216. doi:10.1016/S1474-4422(12)70291-0
2. Villemagne VL, Burnham S, Bourgeat P, et al. Amyloid β deposition, neurodegeneration, and cognitive decline in sporadic Alzheimer's disease: a prospective cohort study. *The Lancet Neurology*. 2013;12(4):357-367. doi:10.1016/S1474-4422(13)70044-9
3. Dean DC, Jerskey BA, Chen K, et al. Brain differences in infants at differential genetic risk for late-onset Alzheimer disease: a cross-sectional imaging study. *JAMA Neurol*. 2014;71(1):11-22. doi:10.1001/jamaneurol.2013.4544
4. Thal DR, Capetillo-Zarate E, Del Tredici K, Braak H. The development of amyloid beta protein deposits in the aged brain. *Sci Aging Knowledge Environ*. 2006;2006(6):re1. doi:10.1126/sageke.2006.6.re1
5. Braak H, Braak E. Neuropathological stageing of Alzheimer-related changes. *Acta Neuropathol*. 1991;82(4):239-259. doi:10.1007/bf00308809
6. Janelidze S, Zetterberg H, Mattsson N, et al. CSF Aβ42/Aβ40 and Aβ42/Aβ38 ratios: better diagnostic markers of Alzheimer disease. *Ann Clin Transl Neurol*. 2016;3(3):154-165. doi:10.1002/acn3.274
7. Ritchie C, Smailagic N, Noel-Storr AH, Ukoumunne O, Ladds EC, Martin S. CSF tau and the CSF tau/ABeta ratio for the diagnosis of Alzheimer's disease dementia and other dementias in people with mild cognitive impairment (MCI). *Cochrane Database Syst Rev*. 2017;3:CD010803. doi:10.1002/14651858.CD010803.pub2
8. Blennow K, Hampel H. CSF markers for incipient Alzheimer's disease. *The Lancet Neurology*. 2003;2(10):605-613. doi:10.1016/s1474-4422(03)00530-1
9. Hampel H, Bürger K, Teipel SJ, Bokde ALW, Zetterberg H, Blennow K. Core candidate neurochemical and imaging biomarkers of Alzheimer's disease. *Alzheimers Dement*. 2008;4(1):38-48. doi:10.1016/j.jalz.2007.08.006
10. Nathan PJ, Lim YY, Abbott R, et al. Association between CSF biomarkers, hippocampal volume and cognitive function in patients with amnestic mild cognitive impairment (MCI). *Neurobiol Aging*. 2017;53:1-10. doi:10.1016/j.neurobiolaging.2017.01.013
11. Selkoe DJ. The molecular pathology of Alzheimer's disease. *Neuron*. 1991;6(4):487-498. doi:10.1016/0896-6273(91)90052-2
12. Hardy JA, Higgins GA. Alzheimer's disease: the amyloid cascade hypothesis. *Science*. 1992;256(5054):184-185. doi:10.1126/science.1566067
13. Reitz C. Alzheimer's disease and the amyloid cascade hypothesis: a critical review. *Int J Alzheimers Dis*. 2012;2012:369808. doi:10.1155/2012/369808
14. Hou Y, Dan X, Babbar M, et al. Ageing as a risk factor for neurodegenerative disease. *Nat Rev Neurol*. 2019;15(10):565-581. doi:10.1038/s41582-019-0244-7
15. Yamazaki Y, Zhao N, Caulfield TR, Liu C-C, Bu G. Apolipoprotein E and Alzheimer disease: pathobiology and targeting strategies. *Nat Rev Neurol*. 2019;15(9):501-518. doi:10.1038/s41582-019-0228-7
16. Prins ND, Scheltens P. White matter hyperintensities, cognitive impairment and dementia: an update. *Nat Rev Neurol*. 2015;11(3):157-165. doi:10.1038/nrneurol.2015.10
17. Yang J, Pan P, Song W, et al. Voxelwise meta-analysis of gray matter anomalies in Alzheimer's disease and mild cognitive impairment using anatomic likelihood estimation. *J Neurol Sci*. 2012;316(1-2):21-29. doi:10.1016/j.jns.2012.02.010

18. Matsuda H. Voxel-based Morphometry of Brain MRI in Normal Aging and Alzheimer's Disease. *Aging and Disease*. 2013;4(1):29-37. Accessed December 2, 2020. https://www.ncbi.nlm.nih.gov/pmc/articles/PMC3570139/
19. A. Armstrong R. A critical analysis of the 'amyloid cascade hypothesis'. *fn*. 2014;3:211-225. doi:10.5114/fn.2014.45562
20. Busche MA, Hyman BT. Synergy between amyloid-β and tau in Alzheimer's disease. *Nat Neurosci*. 2020;23(10):1183-1193. doi:10.1038/s41593-020-0687-6
21. Schöll M, Lockhart SN, Schonhaut DR, et al. PET Imaging of Tau Deposition in the Aging Human Brain. *Neuron*. 2016;89(5):971-982. doi:10.1016/j.neuron.2016.01.028
22. Maass A, Landau S, Baker SL, et al. Comparison of multiple tau-PET measures as biomarkers in aging and Alzheimer's disease. *Neuroimage*. 2017;157:448-463. doi:10.1016/j.neuroimage.2017.05.058
23. Matsuda H. MRI morphometry in Alzheimer's disease. *Ageing Res Rev*. 2016;30:17-24. doi:10.1016/j.arr.2016.01.003
24. Jack CR, Bennett DA, Blennow K, et al. A/T/N: An unbiased descriptive classification scheme for Alzheimer disease biomarkers. *Neurology*. 2016;87(5):539-547. doi:10.1212/WNL.0000000000002923
25. Jack CR, Bennett DA, Blennow K, et al. NIA-AA Research Framework: Toward a biological definition of Alzheimer's disease. *Alzheimers Dement*. 2018;14(4):535-562. doi:10.1016/j.jalz.2018.02.018
26. Soldan A, Pettigrew C, Fagan AM, et al. ATN profiles among cognitively normal individuals and longitudinal cognitive outcomes. *Neurology*. 2019;92(14):e1567-e1579. doi:10.1212/WNL.0000000000007248
27. Altomare D, Wilde A de, Ossenkoppele R, et al. Applying the ATN scheme in a memory clinic population: The ABIDE project. *Neurology*. 2019;93(17):e1635-e1646. doi:10.1212/WNL.0000000000008361
28. van Maurik IS, Vos SJ, Bos I, et al. Biomarker-based prognosis for people with mild cognitive impairment (ABIDE): a modelling study. *The Lancet Neurology*. 2019;18(11):1034-1044. doi:10.1016/S1474-4422(19)30283-2
29. Jack CR, Wiste HJ, Therneau TM, et al. Associations of Amyloid, Tau, and Neurodegeneration Biomarker Profiles With Rates of Memory Decline Among Individuals Without Dementia. *JAMA*. 2019;321(23):2316-2325. doi:10.1001/jama.2019.7437
30. Yu J-T, Li J-Q, Suckling J, et al. Frequency and longitudinal clinical outcomes of Alzheimer's AT(N) biomarker profiles: A longitudinal study. *Alzheimers Dement*. 2019;15(9):1208-1217. doi:10.1016/j.jalz.2019.05.006
31. Guo T, Korman D, Baker SL, Landau SM, Jagust WJ. Longitudinal Cognitive and Biomarker Measurements Support a Unidirectional Pathway in Alzheimer's Disease Pathophysiology. *Biol Psychiatry*. 2020. doi:10.1016/j.biopsych.2020.06.029
32. Tan M-S, Ji X, Li J-Q, et al. Longitudinal trajectories of Alzheimer's ATN biomarkers in elderly persons without dementia. *Alzheimers Res Ther*. 2020;12(1):55. doi:10.1186/s13195-020-00621-6
33. Ekman U, Ferreira D, Westman E. The A/T/N biomarker scheme and patterns of brain atrophy assessed in mild cognitive impairment. *Sci Rep*. 2018;8(1):8431. doi:10.1038/s41598-018-26151-8
34. Jessen F, Spottke A, Boecker H, et al. Design and first baseline data of the DZNE multicenter observational study on predementia Alzheimer's disease (DELCODE). *Alzheimers Res Ther*. 2018;10(1):15. doi:10.1186/s13195-017-0314-2
35. McKhann G, Drachman D, Folstein M, Katzman R, Price D, Stadlan EM. Clinical diagnosis of Alzheimer's disease: report of the NINCDS-ADRDA Work Group under the auspices of Department of Health and Human Services Task Force on Alzheimer's Disease. *Neurology*. 1984;34(7):939-944. doi:10.1212/wnl.34.7.939

945 36. Folstein MF, Folstein SE, McHugh PR. Mini-mental state: A practical method for grading the state of
946 patients for the clinician. *Journal of Psychiatric Research*. 1975;12(3):189-198. doi:10.1016/0022-
947 3956%2875%2990026-6
948 37. Wolfsgruber S, Kleineidam L, Guski J, et al. Minor neuropsychological deficits in patients with
949 subjective cognitive decline. *Neurology*. 2020;95(9):e1134-e1143.
950 doi:10.1212/WNL.0000000000010142
951 38. Wellcome Trust Centre for Human Neuroimaging, University College London. Statistical Parametric
952 Mapping software. Accessed February 8, 2022. https://www.fil.ion.ucl.ac.uk/spm/
953 39. Structural Brain Mapping group, Jena University Hospital. CAT-Toolbox. Accessed February 8, 2022.
954 http://www.neuro.uni-jena.de/cat/
955 40. Rajapakse JC, Giedd JN, Rapoport JL. Statistical approach to segmentation of single-channel cerebral
956 MR images. *IEEE Trans Med Imaging*. 1997;16(2):176-186. doi:10.1109/42.563663
957 41. Ashburner J, Friston KJ. Diffeomorphic registration using geodesic shooting and Gauss-Newton
958 optimisation. *Neuroimage*. 2011;55(3):954-967. doi:10.1016/j.neuroimage.2010.12.049
959 42. Laboratory for Computational Neuroimaging, Massachusetts General Hospital. Freesurfer. Accessed
960 February 8, 2022. http://surfer.nmr.mgh.harvard.edu/
961 43. Fischl B, van der Kouwe A, Destrieux C, et al. Automatically parcellating the human cerebral cortex.
962 *Cereb Cortex*. 2004;14(1):11-22. doi:10.1093/cercor/bhg087
963 44. Fischl B, Salat DH, Busa E, et al. Whole Brain Segmentation. *Neuron*. 2002;33(3):341-355.
964 doi:10.1016/s0896-6273(02)00569-x
965 45. Busatto GF, Diniz BS, Zanetti MV. Voxel-based morphometry in Alzheimer's disease. *Expert Rev*
966 *Neurother*. 2008;8(11):1691-1702. doi:10.1586/14737175.8.11.1691
967 46. Ferreira LK, Diniz BS, Forlenza OV, Busatto GF, Zanetti MV. Neurostructural predictors of Alzheimer's
968 disease: a meta-analysis of VBM studies. *Neurobiol Aging*. 2011;32(10):1733-1741.
969 doi:10.1016/j.neurobiolaging.2009.11.008
970 47. Leandrou S, Petroudi S, Kyriacou PA, Reyes-Aldasoro CC, Pattichis CS. Quantitative MRI Brain Studies
971 in Mild Cognitive Impairment and Alzheimer's Disease: A Methodological Review. *IEEE Rev Biomed*
972 *Eng*. 2018;11:97-111. doi:10.1109/RBME.2018.2796598
973 48. Teipel SJ, Meindl T, Grinberg L, Heinsen H, Hampel H. Novel MRI techniques in the assessment of
974 dementia. *Eur J Nucl Med Mol Imaging*. 2008;35 Suppl 1:S58-69. doi:10.1007/s00259-007-0703-z
975 49. Baker SL, Maass A, Jagust WJ. Considerations and code for partial volume correcting 18F-AV-1451
976 tau PET data. *Data Brief*. 2017;(15):648-657. doi:10.1016/j.dib.2017.10.024
977 50. Iglesias JE, Augustinack JC, Nguyen K, et al. A computational atlas of the hippocampal formation
978 using ex vivo, ultra-high resolution MRI: Application to adaptive segmentation of in vivo MRI.
979 *Neuroimage*. 2015;115:117-137. doi:10.1016/j.neuroimage.2015.04.042
980 51. Koncz R, Sachdev PS. Are the brain's vascular and Alzheimer pathologies additive or interactive? *Curr*
981 *Opin Psychiatry*. 2018;31(2):147-152. doi:10.1097/YCO.0000000000000395
982 52. Roseborough A, Ramirez J, Black SE, Edwards JD. Associations between amyloid β and white matter
983 hyperintensities: A systematic review. *Alzheimers Dement*. 2017;13(10):1154-1167.
984 doi:10.1016/j.jalz.2017.01.026
985 53. Toledo JB, Arnold SE, Raible K, et al. Contribution of cerebrovascular disease in autopsy confirmed
986 neurodegenerative disease cases in the National Alzheimer's Coordinating Centre. *Brain*.
987 2013;136(Pt 9):2697-2706. doi:10.1093/brain/awt188
988 54. Mortamais M, Artero S, Ritchie K. Cerebral white matter hyperintensities in the prediction of
989 cognitive decline and incident dementia. *Int Rev Psychiatry*. 2013;25(6):686-698.
990 doi:10.3109/09540261.2013.838151
991 55. Schmidt P. *Bayesian Inference for Structured Additive Regression Models for Large-Scale Problems*
992 *with Applications Tomedical Imaging: Dissertation an Der Fakultät Für Mathematik, Informatik Und*

Statistik Der Ludwig-Maximilians-Universität München. [Dissertation]: Ludwig-Maximilians-Universität München; 2017. http://nbn-resolving.de/urn:nbn:de:bvb:19-203731

56. Schmidt P. LST. A lesion segmentation tool for SPM. Accessed March 7, 2022. http://www.statistical-modelling.de/lst.html
57. Bertens D, Tijms BM, Scheltens P, Teunissen CE, Visser PJ. Unbiased estimates of cerebrospinal fluid β-amyloid 1-42 cutoffs in a large memory clinic population. *Alzheimers Res Ther*. 2017;9(1):8. doi:10.1186/s13195-016-0233-7
58. Schwarz G. Estimating the Dimension of a Model. *Ann Statist*. 1978;6(2). doi:10.1214/aos/1176344136
59. Hwang J, Jeong JH, Yoon SJ, et al. Clinical and Biomarker Characteristics According to Clinical Spectrum of Alzheimer's Disease (AD) in the Validation Cohort of Korean Brain Aging Study for the Early Diagnosis and Prediction of AD. *J Clin Med*. 2019;8(3). doi:10.3390/jcm8030341
60. Burnham SC, Coloma PM, Li Q-X, et al. Application of the NIA-AA Research Framework: Towards a Biological Definition of Alzheimer's Disease Using Cerebrospinal Fluid Biomarkers in the AIBL Study. *J Prev Alzheimers Dis*. 2019;6(4):248-255. doi:10.14283/jpad.2019.25
61. Grøntvedt GR, Lauridsen C, Berge G, et al. The Amyloid, Tau, and Neurodegeneration (A/T/N) Classification Applied to a Clinical Research Cohort with Long-Term Follow-Up. *J Alzheimers Dis*. 2020;74(3):829-837. doi:10.3233/JAD-191227
62. Kakeda S, Korogi Y. The efficacy of a voxel-based morphometry on the analysis of imaging in schizophrenia, temporal lobe epilepsy, and Alzheimer's disease/mild cognitive impairment: a review. *Neuroradiology*. 2010;52(8):711-721. doi:10.1007/s00234-010-0717-2
63. Karas GB, Scheltens P, Rombouts SARB, et al. Global and local gray matter loss in mild cognitive impairment and Alzheimer's disease. *Neuroimage*. 2004;23(2):708-716. doi:10.1016/j.neuroimage.2004.07.006
64. Chételat G, Landeau B, Eustache F, et al. Using voxel-based morphometry to map the structural changes associated with rapid conversion in MCI: a longitudinal MRI study. *Neuroimage*. 2005;27(4):934-946. doi:10.1016/j.neuroimage.2005.05.015
65. Pini L, Pievani M, Bocchetta M, et al. Brain atrophy in Alzheimer's Disease and aging. *Ageing Res Rev*. 2016;30:25-48. doi:10.1016/j.arr.2016.01.002
66. Baron JC, Chételat G, Desgranges B, et al. In vivo mapping of gray matter loss with voxel-based morphometry in mild Alzheimer's disease. *Neuroimage*. 2001;14(2):298-309. doi:10.1006/nimg.2001.0848
67. Ramos Bernardes da Silva Filho S, Oliveira Barbosa JH, Rondinoni C, et al. Neuro-degeneration profile of Alzheimer's patients: A brain morphometry study. *Neuroimage Clin*. 2017;15:15-24. doi:10.1016/j.nicl.2017.04.001
68. Zanchi D, Giannakopoulos P, Borgwardt S, Rodriguez C, Haller S. Hippocampal and Amygdala Gray Matter Loss in Elderly Controls with Subtle Cognitive Decline. *Front Aging Neurosci*. 2017;9:50. doi:10.3389/fnagi.2017.00050
69. Jones BF, Barnes J, Uylings HBM, et al. Differential regional atrophy of the cingulate gyrus in Alzheimer disease: a volumetric MRI study. *Cereb Cortex*. 2006;16(12):1701-1708. doi:10.1093/cercor/bhj105
70. Kumar D, Ganeshpurkar A, Kumar D, Modi G, Gupta SK, Singh SK. Secretase inhibitors for the treatment of Alzheimer's disease: Long road ahead. *Eur J Med Chem*. 2018;148:436-452. doi:10.1016/j.ejmech.2018.02.035
71. van Dyck CH. Anti-Amyloid-β Monoclonal Antibodies for Alzheimer's Disease: Pitfalls and Promise. *Biol Psychiatry*. 2018;83(4):311-319. doi:10.1016/j.biopsych.2017.08.010

72. Masliah E, Mallory M, Hansen L, Richard D, Alford M, Terry R. Synaptic and neuritic alterations during the progression of Alzheimer's disease. *Neuroscience Letters*. 1994;174(1):67-72. doi:10.1016/0304-3940(94)90121-X
73. Knowles RB, Gomez-Isla T, Hyman BT. Abeta associated neuropil changes: correlation with neuronal loss and dementia. *J Neuropathol Exp Neurol*. 1998;57(12):1122-1130. doi:10.1097/00005072-199812000-00003
74. Fortea J, Vilaplana E, Alcolea D, et al. Cerebrospinal fluid β-amyloid and phospho-tau biomarker interactions affecting brain structure in preclinical Alzheimer disease. *Ann Neurol*. 2014;76(2):223-230. doi:10.1002/ana.24186
75. Montal V, Vilaplana E, Alcolea D, et al. Cortical microstructural changes along the Alzheimer's disease continuum. *Alzheimer's & Dementia*. 2018;14(3):340-351. doi:10.1016/j.jalz.2017.09.013
76. Stern Y, Arenaza-Urquijo EM, Bartrés-Faz D, et al. Whitepaper: Defining and investigating cognitive reserve, brain reserve, and brain maintenance. *Alzheimer's & Dementia*. 2020;16(9):1305-1311. doi:10.1016/j.jalz.2018.07.219
77. Ingala S, Boer C de, Masselink LA, et al. Application of the ATN classification scheme in a population without dementia: Findings from the EPAD cohort. *Alzheimer's & Dementia*. 2021;17(7):1189-1204. doi:10.1002/alz.12292
78. Nelson PT, Abner EL, Patel E, et al. The Amygdala as a Locus of Pathologic Misfolding in Neurodegenerative Diseases. *J Neuropathol Exp Neurol*. 2018;77(1):2-20. doi:10.1093/jnen/nlx099
79. Mattsson-Carlgren N, Leuzy A, Janelidze S, et al. The implications of different approaches to define AT(N) in Alzheimer disease. *Neurology*. 2020;94(21):e2233-e2244. doi:10.1212/WNL.0000000000009485
80. Illán-Gala I, Pegueroles J, Montal V, et al. Challenges associated with biomarker-based classification systems for Alzheimer's disease. *Alzheimers Dement (Amst)*. 2018;10:346-357. doi:10.1016/j.dadm.2018.03.004